Biosensors and Bioelectronics 44 (2013) 89–94

Contents lists available at SciVerse ScienceDirect

Biosensors and Bioelectronics

journal homepage: www.elsevier.com/locate/bios

Porous silicon optical microcavity biosensor on silicon-on-insulator wafer for sensitive DNA detection

Hongyan Zhang [a], Zhenhong Jia [b,*], Xiaoyi Lv [b], Jun Zhou [c], Liangliang Chen [d], Rongxia Liu [a], Ji Ma [d]

[a] School of Physical Science and Technology, Xinjiang University, Urumqi 830046, PR China
[b] Colleges of Information Science and Engineering, Xinjiang University, Urumqi 830046, PR China
[c] Department of Physics, Ningbo University, Ningbo 315211, PR China
[d] Key Laboratory of Xinjiang Biological Resources and Gene Engineering, College of Life Sciences and Technology, Xinjiang University, Urumqi 830046, PR China

ARTICLE INFO

Article history:
Received 31 October 2012
Received in revised form
6 January 2013
Accepted 7 January 2013
Available online 16 January 2013

Keywords:
Silicon-on-insulator wafer
Porous silicon microcavity
DNA biosensor
High sensitivity

ABSTRACT

Silicon-on-insulator (SOI) wafer is one of the most appealing platforms for optical integrated circuit with the potential to realize high performance Ultra Large Scale Integration (ULSI) and device miniaturization. In this work, based on simulations to obtain appropriate optical properties of a porous silicon microcavity (PSM), we successfully fabricated a highly efficient PSM on SOI wafer by electrochemical etching for DNA detection at optical wavelength 1555.0 nm. The narrow resonance peak with a full width at half maximum about 26.0 nm in the reflectance spectrum gives a high Q factor which causes high sensitivity for sensing performance. The sensitivity of this sensor is investigated through 19-base pair DNA hybridization in the PSM by surface modification using a standard cross link chemistry method. The red shift of the reflectance spectra shows a good linear relationship with complementary DNA concentration, ranging from 0.625 to 12.500 μM, and the detection limit is 43.9 nM. This optical PSM on SOI is highly sensitive, fast responsive, easy to fabricate and low-costly, that will broadly benefit to develop a new optical label-free biosensor on SOI wafer and has a great potential for biochips based on integrated optical devices.

1. Introduction

Biomolecule detection is important for many potential applications including medical diagnostics, food safety and monitoring of the environment (Loncarica et al., 2012; Ercolea et al., 2003; Ricciardi et al., 2010). Label-free biosensors can directly measure unmodified samples as they do not require the use of reporter molecules to generate a signal. To increase the accuracy and efficiency of label-free biosensor, several methods have been developed. For example, the resonance elastic light scattering (RELS) from molecules and nanoparticles results from the absorption of photons followed by an immediate coherent re-emission of light in all directions without any energy loss, that can be used for analytical determination of complexes and biocompounds (Stobiecka and Hepel, 2011; Stobiecka and Hepel, 2010; Stobiecka et al., 2010a; Stobiecka et al., 2010b). Photoluminescence (PL) of epitaxial quantum (QD) could be used to study biochemical reactions on surfaces of semiconductors (Duplan et al., 2011). Surface enhance Raman scattering (SERS) is a surface sensitive optical tool for single molecule detection (Fang et al., 2008). Recently, many label-free optical biosensors based on porous silicon (PS) material have been widely investigated (Hiraoui et al., 2012; Qiao et al., 2010). PS is cheap and easy to obtain and its large internal surface area (up to 800 m^2/g) (Hasar et al., 2012) allows immobilization of more probe molecules which increases the possibility of capturing low concentration target molecules in solution. In particular, PS is widely used for DNA detection, because DNA is the programmable long polymeric network constituting the genetic material of cell and has become popular in biotechnology diagnostics and clinical analysis owing to its inherent molecular recognition property. For example, PS has been used as an optical interferometric transducer for detection small organic molecules and 16-nucleotide DNA oligomers (Lin et al., 1997). Moreover, Photonic crystals (PhCs) made of PS have been used for sensor application. PhCs are attracting attention due to the dielectric functions being periodically modulated, resulting in light propagation dramatically different from the bulk material (Meade et al., 1993; Yablonovitch, 1993), such as photonic bandgap and defect mode, where the former causes the range of frequency in which optical propagation is prohibited in any

* Corresponding author. Tel.: +86 0991 858 3362.
E-mail address: jzhh@xju.edu.cn (Z. Jia).

0956-5663/$ - see front matter © 2013 Elsevier B.V. All rights reserved.
http://dx.doi.org/10.1016/j.bios.2013.01.012

direction and the latter allows modes to appear in photonic bandgap which is localized within a small volume around the defect. In general, they are more compact and more sensitive than other devices. Since the first biosensor on the photonic crystal platform, many groups have been working with different PhCs sensor architectures to demonstrate higher sensitivity (Lv et al., 2011; Jamois et al., 2010; Huanca et al., 2008). Among them, PSM is especially investigated due to its strong field-confining ability and promising architecture to achieve highly sensitive biosensors. A survey of the literatures shows that these research groups have used PSM to biological molecule detection (Li et al., 2011; Suaŕez et al., 2012).

Although these optical biosensors are easy to be used, capable of rapidity, selective and sensitive for biomolecule detection, they are still limited in integrated optical devices. When a PhCs has a symmetric structure in vertical direction, like air-bridge structure with air cladding on both sides, such a structure is mechanically unstable from practical perspective and yet not suitable for ULSI. But for asymmetrical structure, like SOI structures with silicon epitaxial layer between SiO_2 layer cladding on one side and air cladding on other side, the above instability can be overcome. Therefore SOI technology has been considered to be one of the most promising techniques to realize high performance ULSI with low power consumption and high carrier mobility (Settle et al., 2006). It is possible to produce significantly miniaturized devices by integrating the biosensor and Si electronic circuits of preamplifier on the same SOI substrate. Moreover, SOI wafer is one of the most appealing platforms for optical integrated circuit, due to the lightly doped Si-overlayer being transparent for telecom wavelengths and ensuring effective mode confinement. So SOI platforms are commonly adopted to develop optical devices including waveguides, filters, switches, variable attenuators and modulators (Quan et al., 2008; Wang et al., 2009; Jia et al., 2008; Thomas et al., 2011). However, their fabrication is in general complicated and high-costly. So far, few papers have been reported about PS based on SOI wafer by electrochemical anodization (Zhong et al., 2012), which is simple and low-costly.

In the present study, through electrochemical etching, we firstly fabricated a PSM on SOI wafer by controlling alternate low-level and high-level current density and etching time in the anodization process. This optical PSM biosensor on SOI wafer has a high value of the Q factor for DNA detection by surface modification, which is simple, rapid, sensitive, and low-costly. Moreover the optical wavelength of the narrow resonance peak of the reflectance spectrum is about 1550.0 nm, which is well-known one of the working wavelengths in optical communication, and the preparation technology of optical devices working at this wavelength is very mature. Therefore the present research provides an interesting way to develop a new optical label-free biosensor on SOI wafer and has great potential for biochips based on integrated optical devices.

2. Theory and Experiment

2.1. Theory

From an optical point of view, a PSM is constituted of a Fabry–Perot cavity between two Bragg reflectors (DBRs). Each DBR is composed of a periodic multilayer structures of PS films. The optical characteristic of this structure is of high reflectivity stop band with one narrow resonance peak of transmittance approximately in its center. In order to obtain the photonic band-gap feature and the maximum value of the reflectance spectrum, by changing the current density in the anodization process, we can obtain the low (L) and high (H) refractive index layers. Thus, the reflectance maximum appears at Bragg wavelengths (λ_{Bragg}) satisfying the following relation,

$$\frac{m\lambda_{Bragg}}{2} = n_L d_L + n_H d_H$$

where m is a positive integer, n_L and n_H are refractive indexes of single PS layer, and d_L and d_H are the thicknesses of low refractive index (n_L) and high refractive index layer (n_H), respectively. The multiplied terms, $n_L d_L$ and $n_H d_H$, are the optical thicknesses of low refractive index layer (n_L) and high refractive one (n_H). The position of the narrow resonance peak of transmittance is determined by the optical thickness. In this study, the DBRs are constructed with several periods of high and low porosity layers with an effective optical thickness of $\lambda/4$ for each DBR layer and λ for the central layer.

When PSM is exposed to the DNA solution, small molecules attach to PS layers, which causes a red shift in the reflectance spectrum due to the change of the optical thickness. In fact, the adsorbed molecules on the walls cause an increase in the average refractive index of the PS, and hence its characteristic peak shifts toward to longer wavelength.

2.2. Preparation of PSM on SOI Wafer

The PSM structures were obtained from the SOI wafer, consisting of 60 μm thick p-type (100) silicon epitaxial layer with a resistivity of 0.01–0.02 Ω cm, and grown on 2.0 μm thick buried oxide layer on 420 μm thick p-type (100) silicon substrate, under the electrochemical anodization process in the mixed solution composed of 49% aqueous hydrofluoric acid and ethanol with the volume ratio of 1:1. In the teflon electrochemical etch cell, the saturated salt water was an anode as a counter electrode and the copper was the cathode (Zhong et al., 2012), with an exposing area approximately to 0.785 cm^2 to the mixed solution. The Fabry–Perot cavity was obtained by the $(HL)^p HL_c H(LH)^q$ sequence, fabricated from left to right following this sequence and from top down to SOI wafer, where"H" and "L" represent different refractive index layer, "p" and "q" denote the numbers of "H" layer and "L" layer, respectively, and "L_c" layer corresponds to microcavity layer. In order to obtain two DBRs PS layers on the SOI wafer, the periodic multilayer structures of PS films were fabricated by using a computer program (Labview) to alternately change the current density and etching time of anodization process current with 20 mA/cm^2 of 4.9 s for "H" layer, 80 mA/cm^2 of 3.3 s for "L" layer, and 80 mA/cm^2 of 12.1 s for "L_c" layer, and a 3 s pause after each layer formation. In the fabrication process of PSM layer on SOI wafer, the roughness between the layers in the transverse dimension of the cavity affects the spectral properties of the Fabry–Perot cavity, and the enhancement of light scattering at the rough interface causes a low reflectance value. Therefore, to ensure good homogeneity of the skeleton, stable ambient temperature was also guaranteed to achieve high repeatability with all the steps performed under strict-controlled conditions. So the electrolyte temperature was maintained at 2 °C for the duration of the reaction in order to reduce the roughness of the surface interface.

2.3. Functionalization of PSM on the SOI Wafer

2.3.1. Materials and Characterizations

3-Aminopropyltriethoxysilane (APTES), glutaraldehyde (50%, GA), ethanolamine (EA) and 4-(2-Hydroxyethyl)-1-piperazineethanesulfonic acid (HEPES) used in this experiment were purchased from Aladdin Reagen Co. (China, 〈www.aladdin-reagent.com〉). The physical thickness of one APTES monolayer and the total thickness of the APTES+GA layer were determined to be 0.8 ± 0.11 nm and

1.5 ± 0.1 nm, respectively (Ouyang et al., 2006; Wei and Weiss 2011). The DNA was prepared by the Key Laboratory of Xinjiang Biological Resources and Gene Engineering. The sequences of probe DNA, complementary DNA, and non-complementary DNA are 5′-TTGTACAGCAGCGTGCACC-3′ (19-base), 5′-GGTGCACGCTGCTGTACAA-3′ (19-base), and 5′-ACACGTCATCGCTCTATTG-3′ (19-base), respectively, and the length of them are the same as about 4 nm.

Measurement of thickness and configuration of the nanopores of PSM on SOI wafers were carried out with ZEISS SUPRA 55VP (Zeiss SMT, Germany) Field Emission Electron Microscope (FSEM). The reflectivity spectra of the sample were taken by UV–vis spectrophotometer (Hitachi U-4100, Japan) in the wavelength range from 400.0 to 2000.0 nm.

2.3.2. Oxidization

The freshly etched PS is unstable in the air owing to the "fragile" Si–H bond easily to be oxidized, so PSM surface needs to be stabilized before the immobilization. To do this, the prepared PSM on SOI wafer was soaked in H_2O_2 (30%) for 24 h at room temperature. Then the wafers were rinsed with deionized water and dried in the air. Due to the existence of Si–O–Si, O–Si–H, O_3–Si–H groups and bridging of inter-atomic silicon layers with O atoms, the PSM becomes stable. In addition to stabilization, oxidation of PS also introduces hydrophilicity to the material which is an essential requirement in biological application.

2.3.3. Silanization

The prepared PSM wafers were dipped into 5% solution of APTES in water/methanol mixture (v/v=1:1) for 1 h at room temperature. In order to promote cross-linking and remove excess solvent, the resulting wafers were then rinsed with deionized water and heated at 100 °C for 10 min. After that, the wafers were incubated in 2.5% solution of GA for 1 h at room temperature. Finally, the PSM wafers had to be washed three times with buffer (pH: 7.4) in order to remove all excess of GA.

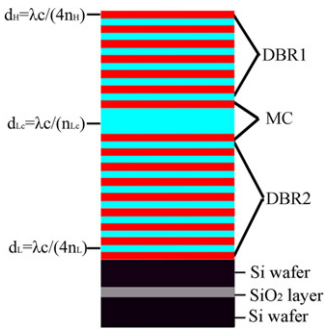

Fig. 1. Scheme of the diagram and parameters of PSM structures.

2.3.4. Immobilization

50 μL probe DNA was dropped onto the prepared PSM wafers at 37 °C for 2 h and the wafers were rinsed with buffer to remove all excess of DNA to prevent non-specific absorption. After that, the wafers were dipped into a 3 M ethanolamine in buffer with PH 9.0 for 1 h at 37 °C, followed by buffer rinse to remove excess ethanolamine and dried in the air.

2.3.5. Detection

The PSM wafers were exposed to solutions with the different concentration of complementary DNA, then washed with buffer to remove the excessive complementary DNA and dried in the air.

3. Results and Discussions

In order to obtain the proper PSM on the SOI wafer with high sensitivity, the following three factors were taken into account: firstly, a proper number of layers of the fabricated PSM is expected because the anisotropy of the etching rate during the PS formation increases as it goes to deeper, which destroys the homogeneity of the PSM' skeleton. Secondly, the pore size is large enough to permit biomolecules to infiltrate into PSM. Lastly, it is important to allow more biomolecules to enter the cavity of PSM in order to improve the sensitivity. The quality factor ($Q=\lambda/\Delta\lambda$) of the microcavity is very important for detecting biomolecule, because a higher Q implies that the light is trapped for a longer period of time in the cavity and hence there is a longer interaction for the light with analyte in the vicinity of the PSM.

Under these considerations, we successfully produced a PSM on the SOI wafer. The PSM structure with parameters is shown in Fig. 1, where it was clear that DBR1 and DBR2 were respectively comprised of six and eight periods of alternating high and low porosity in each stack. In order to determine the optical parameters of the PSM, simulations of the reflectance spectrum had been performed before experiment. The PSM $(HL)^6HL_cH(LH)^8$ sequence was calculated in Fig. 2a using the transfer matrix method, where "H", "L" and "L_c" represent different refractive index layer, with "H" denoting high refractive index layer, "L" and "L_c" denoting the low refractive index layer and the microcavity layer. The resolution of the grid in the digital simulation of reflectance spectrum was set to be 1 nm. The reflective indexes were determined to be $n_H=2.00$, $n_L=n_{Lc}=1.65$ by experiment, and the layer thicknesses corresponding to the reflective indexes were $d_H=\lambda_c/(4n_H)=194.4$ nm and $d_L=\lambda_c/(4n_L)=235.6$ nm, respectively, and the thickness of microcavity was $d_{Lc}=\lambda_c/(n_{Lc})=942.0$ nm, with "λ_c" denoting the resonance wavelength at 1550.0 nm. From Fig. 2b, we can see a sharp resonant peak of PSM at 1555.0 nm appeared in the experimentally measured reflectance spectrum for the freshly etched PSM on SOI wafer, which is in good agreement with the calculated resonance peak of reflectance spectrum. The experimentally measured reflectance spectrum

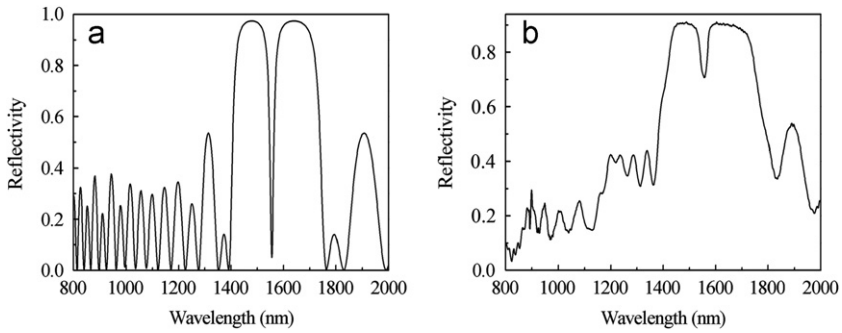

Fig. 2. (a) Calculated reflectance spectrum of PSM structure following the $(HL)^6HL_cH(LH)^8$ sequence. (b) Experimentally measured reflectance spectrum with the same sequence.

shows all the important spectral features. The region of high reflectivity (Bragg plateau) is about 310.0 nm wide for this PSM on SOI wafer and the resonance dip in the reflectance spectrum is very sharp with the full width at half maximum (FWHM) of 26.0 nm which means that the sensor gives a higher Q factor. There are differences between the calculated and the measured reflectance spectra, and we think these differences may come from the following factors, including non-equal surface current density, impurities inside the SOI wafer, some fabrication tolerance, and some loss present inside the cavity. These factors affect the refractive index and thickness of layer in PSM fabrication.

Fig. 3a describes a cross-sectional image of the PSM layer sample. The dark gray color layers correspond to PS layer of high porosity, or low refractive index (n_L), whereas the light gray color layers correspond to the layer of low porosity, or high refractive index (n_H). The overall thickness of PSM layer on the SOI wafer is approximately 7.3 μm, the thickness of high porosity layer is about 240.0 nm and the thickness of low porosity layer is about 190.0 nm. We can see the strong contrast between the alternate layers of the PSM which confirms that a large porosity difference has been achieved. Fig. 3b shows the corresponding detailed cross-section of the PSM. The nanocrystals are sparse and directional for the case of the high porosity layer, the wire-like structures are more isolated while the nanocrystals are more densely packed as a result of their larger size for the low porosity layer. Fig. 3c shows a surface image of the PSM layer on SOI wafer. The average diameter of the pores is approximately 20 nm and the pore distribution is random, which permits biomolecule infiltration. Therefore the PSM has good capability for subsequent small molecule attachment.

Fig. 4 shows the schematic of each functionalization step and the probe DNA conjugation. Oxidized PSM with Si–O–Si surface functionality reacts with APTES. In some cases APTES attached to PSM film reacts further with GA, and subsequent GA tagged films covalently attach with probe DNA. The chemical modification carried out though linker attachment is easier and simple. In order to confirm chemical attachment, we used UV–vis spectrophotometer to measure each functionalization step. Fig. 5a shows the reflectance spectra for each functionalization step (from left to right): after oxidation process (oxidized), after silanization process (silanized) and after GA. After the modification with APTES, PSM was functionalized with GA. The resulting reflectance spectra demonstrate that there is a remarkable red shift of 36.0 nm observed due to the increase of the refractive index of the PS layer. Usually the effective index depends on several factors, including the molecule concentration, the refractive index of the molecule, exposure time and the diameter of the pore. The red-shifted reflectance in our experiment suggests that the small organic molecules be coupled well together and thus the functionalization has been carried out successfully. Fig. 5b demonstrates the detection of DNA in PSM on SOI wafer, where the resonant peak of PSM red shift is 41.0 nm after the PSM being exposed to the 25.000 μm of complementary DNA. When the immobilized probe DNA in the pores of PSM is exposed to the complementary DNA, the two DNAs hybridization increases the effective refractive index of the PS layer, and thus causes a red shift of the resonance peak. Controlled experiments were performed on PSM on SOI wafer to demonstrate selectivity. Fig. 5c and d show the PSM exposure to 50.000 μm non-complementary DNA and buffer solution separately. Since the probe DNA and non-complementary DNA do not bind in the pores of the PSM, the refractive index keeps unchanged and thus causes no shift of the resonance peak. We note that there are negligible shifts in detected spectra after immersion in non-complementary DNA and buffer solution. We think that there is no one-to-one correspondence between fabrication process and measured spectral properties of PSM on SOI wafer (Hasar et al., 2012). Although there is no such correspondence, the variation of resonance wavelength is very slight. Therefore the negligible shifts of the resonance peak in Fig. 5c and 5d indicate that PSM on SOI wafer is able to select DNA hybridization between complementary and non-complementary DNA.

The red shift of the reflectance quantifies the DNA concentration. We expect that the ultimate detection limit is much smaller than 50.000 μm. Fig. 6 shows the red shift of the reflectance resonant peak for 19-base complementary DNA at different concentrations (i.e. 0.3125, 0.625, 1.250, 2.500, 3.125, 6.250, 10.000, 12.500, 25.000 and 50.000 μm). Fig. 6 also indicates that the shift values of the resonant peak are related to the concentrations of the complementary

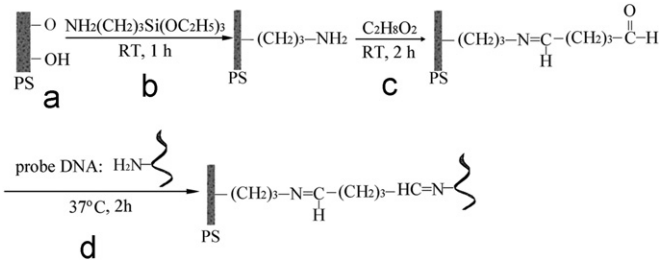

Fig. 4. Schematic of (a) oxidized PSM, (b) silanization process, (c) glutaraldehyde process and (d) probe DNA conjugation.

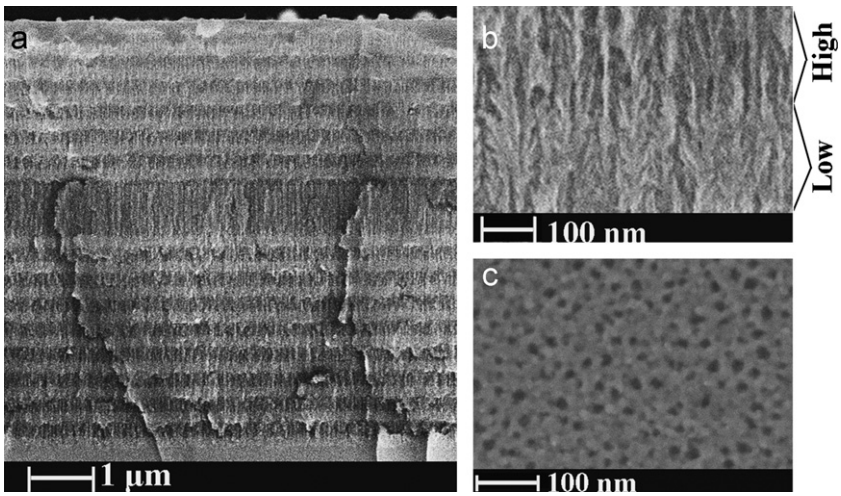

Fig. 3. (a) SEM cross section image of the PSM, (b) Detailed cross section image of the PSM and (c) Top view of the surface.

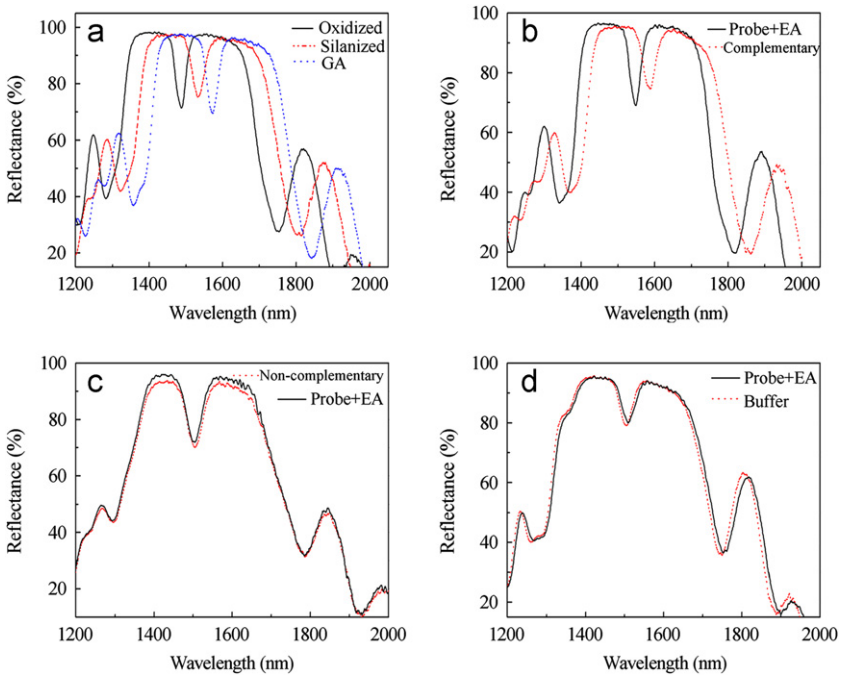

Fig. 5. (a) Reflectance spectra of PSM after oxidization, after silanization and after glutaraldehyde treatment. (b) Resonance shift of PSM for complementary DNA (25 μm). (c) Negligible resonance shift of PSM for non-complementary DNA. (d) No resonance shift of PSM on exposure to buffer solution.

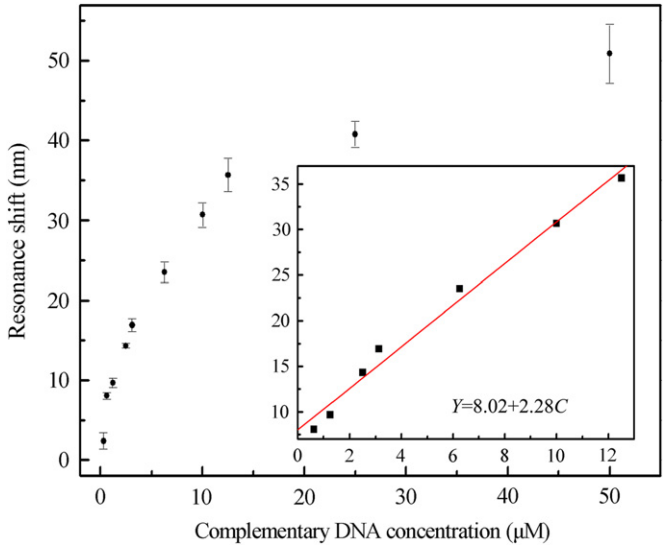

Fig. 6. Red shift of the resonance during exposure of the PSM to different concentration of DNA from 0.3125 to 50.000 μM, and the inset shows the fitted linear relation to the DNA concentration ranging from 0.625 to 10.000 μM.

DNA and the red shifts corresponding to these concentrations are 2.83, 8.06, 9.67, 14.33, 16.93, 23.53, 30.67, 35.67 40.77 and 50.90 nm, respectively. The linearity of the red shift of the reflectance spectrum as a function of the concentration of complementary DNA in the range from 0.625 to 12.500 μm is also shown in inset of Fig. 6. The linear equation is $Y=8.02+2.28C$ and the correlation coefficient is 0.993, where Y represents the red shift of the resonance peak and C represents the concentration of complementary DNA. Therefore, the sensitivity of the sensor is 2.28 nM/μM calculated by the slope. With the resolution 0.1 nm of the UV–vis spectrophotometer, the ultimate detection limit of the PSM on SOI biosensor is $0.1/2.28=43.9$ nM. The reproducibility of the DNA sensor has been undertaken in triplicate between three samples under the same condition. Experimental data, Error bars, standard deviations (s) and relative standard deviations (RSD) are given in the supplementary material (Table 1s). The DNA detection limit based on PSM biosensor used SOI as a wafer is of nM concentration, which is comparable to that reported for other favorable PS biosensor techniques based on silicon as a wafer, such as novel PS polybasic symmetrical structure for detecting 23-base pair DNA with the limit of 21.3 nM (Lv et al., 2013) and PS membrane waveguide for 24-base pair DNA with the limit of 42.0 nM (Rong et al., 2008). Considering that the fabricated process on SOI wafer by electrochemical etching is easy and low-costly, this research could be interesting to develop a new optical label-free biosensor on SOI wafer.

In this work, we tested 19-base DNA sequence in an ideal condition. However, real sample from patients can have impurities, which might affect accuracy of detection. In order to verify the effectiveness of the biosensor for single base mismatch DNA detection, we used a single base mismatch DNA. The sequence for probe DNA is 5′-TTGTACAGCAGCGTGCACC-3′ (19-base) and for single base mismatch DNA is 5′-GGTGCACGCTGCTGTACAC-3′ (19-base). The results show there still is a red shift of the reflectance spectra of the PSM on SOI wafer. The linear fitness of the experimental data is given as supplementary materials (Figs. 1S and 2S). That means this technique can also distinct single base mismatch from the difference between the red shifts of the resonance peaks. Compared with the detection of complementary DNA in Figs. 5 and 6, the red shift of single base mismatch DNA is smaller, and the sensitivity for this case is lower. So given either complementary DNA or single base mismatch DNA, this technique can be used to detect the concentration of the target DNA.

4. Conclusions

Biosensor based on SOI wafer is well suited for high performance and device miniaturization. Considering the well-known optical wavelength at 1550 nm, we optimized the PSM biosensor performance through simulations and experiments to determine the experimentally measured resonance peak at 1555 nm. A sharp resonance peak in the reflectance spectrum shows a high Q factor. 19-base DNA oligonucleotides are immobilized in functionalized

PSM pores by standard cross-link chemistry method. Our results indicate that the red shift comes from the refractive index changes induced by the DNA hybridization in the pores of the PSM. The red shift of the resonance peak of PSM on SOI wafer is linearly correlated with the concentration of complementary DNA, ranging from 0.625 to 12.500 μm with a detection limit of 43.9 nm. As it is high sensitive, fast response and low-costly, the optical PSM based on SOI wafer is promising in biomolecule detection and has a great potential for biochips based on integrated optical devices.

Acknowledgments

This work was supported by the National Science Foundation of China (No. 60968002 and 61265009), Research Foundation for the Doctoral Program of Chinese Universities (No. 20116501110003), and Xinjiang Science and Technology Project (No. 201291109 and 2012211B01).

Appendix A. Supporting information

Supplementary data associated with this article can be found in the online version at http://dx.doi.org/0.1016/j.bios.2013.01.012.

References

Duplan, V., Frost, E., Dubowski, J.J., 2011. Sensors and Actuators B 160, 46–51.
Ercolea, C., Gallo, M., Mosiello, M.D., Baccella, L., Lepidi, A., S., 2003. Sensors and Actuators B 91, 163–168.
Fang, C., Agarwal, A., Buddharaju, K.D., Khalid, N.M., Salim, S.M., Widjaja, E., Garland, M., Balasubramanian, N., Kwong, D., 2008. Biosensors and Bioelectronics 24, 216–221.
Hasar, U.C., Ozbek, I.Y., Oral, E.A., Karacali, T., Efeoglu, H., 2012. Optics Express 20, 22208–22223.
Hiraoui, M., Haji, L., Guendouz, M., Lorrain, N., Moadhen, A., Oueslati, M., 2012. Biosensors and Bioelectronics 36, 212–216.
Huanca, D.R., Ramirez-Fernandez, F.J., Salcedo, W.J., 2008. Microelectronics Journal 39, 499–506.
Jamois, C., Li, C., Orobtchouk, R., Benyattou, T., 2010. Photonics and Nanostructures—Fundamentals and Applications 8, 72–77.
Jia, X.L., Luo, S.Q., Cheng, X.H., 2008. Optics Communications 281, 1003–1007.
Loncarica, C., Tang, Y.T., Ho, C., Parameswaran, M.A., Yu, H.Z., 2012. Sensors and Actuators B 161, 908–913.
Li, S., Huang, J.F., Cai, L.T., 2011. Nanotechnology 22 (425502), 1–6.
Lin, V.S., Motesharei, K., Dancil, K.P., Ghadiri, M.R., 1997. Science (New York, NY) 278, 840–843.
Lv, X.Y., Mo, J.Q., Jiang, T, Zhong, F.R., Jia, Z.H., Li, J.W., Zhang, F.C., 2011. Applied Surface Science 257, 1906–1910.
Lv, X.Y., Chen, L.L., Zhang, H.Y., Mo, J.Q., Zhong, F.R., Lv, C.W., Ma, J., Jia, Z.H., 2013. Biosensors and Bioelectronics 39, 329–333.
Meade, R.D., Rappe, A.M., Brommer, K.D., Joannopoulos, J.D., 1993. Physical Review B 48, 8434–8437.
Ouyang, H.M., Striemer, C.C., Fauchet, P.M., 2006. Applied Physics Letters 88 (163108), 1–3.
Qiao, H., Guan, Bin., Gooding, J.J., Reece, P.J., 2010. Optics Express 18, 15174–15182.
Quan, Y.J., Han, P.D., Ran, Q.J., Zeng, F.P., Gao, L.P., Zhao, C.H., 2008. Optics Communications 281, 3105–3110.
Ricciardi, C., Canavese, G., Castagna, R., Ferrante, I., Ricci, A., Marasso, S.L., Napione, L., Bussolino, F., 2010. Biosensors and Bioelectronics 26, 1565–1570.
Rong, G.G., Ryckman, J.D., Mernaugh, R.L., Weiss, S.M., 2008. Applied Physics Letters 93 (161109), 1–3.
Settle, M., Salib, M., Michaeli, A., Krauss, T.F., 2006. Optics Express 14, 2440–2445.
Stobiecka, M., Hepel, M., 2010. Sensors and Actuators B 149, 373–380.
Stobiecka, M., Hepel, M., 2011. Biomaterials 32, 3312–3321.
Stobiecka, M., Coopersmith, K., Hepel, M., 2010a. Journal of Colloid and Interface Science 350, 168–177.
Stobiecka, M., Deeb, J., Hepel, Maria, 2010b. Biophysical Chemistry 146, 98–107.
Suaŕez, I., Chirvony, V., Hill, D., Martínez-Pastor, J., 2012. Photonics and Nanostructures—Fundamentals and Applications 10, 304–311.
Thomas, R., Ikoni, Z., Kelsall, R.W., 2011. Photonics and Nanostructures—Fundamentals and Applications 9, 101–107.
Wang, T., Zhang, Z.Y., Liu, F.F., Tong, Y., Wang, J., Tian, Y., Qiu, M., Su, Y.K., 2009. Optics Communications 282, 3464–3467.
Wei, X., Weiss, S.M., 2011. Optics Express 19, 11330–11339.
Yablonovitch, E., 1993. Journal of the Optical Society of America B 10, 283–294.
Zhong, F.R., Lv, X.Y., Jia, Z.H., Mo, J.Q., 2012. Optical Engineering 51 (040502), 1–3.